Effect of Drying Rate on Shrinkage of Alkali-Activated Slag Cements

Hailong Ye, Christopher Cartwright, Farshad Rajabipour, and Aleksandra Radlińska
Department of Civil and Environmental Engineering, The Pennsylvania State University

ABSTRACT

The volumetric instability of alkali-activated slag (AAS) binders has raised concerns and impeded the acceptance of this Portland cement-free material. The objective of this article is to characterize the influence of drying rate on drying shrinkage behavior of AAS mortars to better understand the mechanisms responsible for its large shrinkage deformation. A series of four AAS mortar mixtures with varying activator composition, as well as a reference Portland cement mortar, was cast and dried at different relative humidities, that is, 30, 50, 70, and 85% RH. Drying took place inside nitrogen-purged environmental chambers for the purpose of eliminating the contribution of carbonation to the total volumetric change of AAS. The shrinkage and corresponding mass loss of 1.27 cm × 1.27 cm × 12.7 cm prisms were measured as a function of time. The results show that shrinkage of AAS varies largely depending on the drying rate, that is, ambient RH. Interestingly, even though the drying mass loss increases with reducing the RH, the magnitude of shrinkage is the largest for samples stored at 50 and 70% RH, depending on the mixture type. Possible causes of these irregular behaviors are discussed. It is concluded that the drying rate has a much more significant influence on AAS than on ordinary Portland cement (OPC), which implies a more complicated shrinkage mechanism for AAS samples stored at various relative humidities.

1. INTRODUCTION

Ground-granulated blast furnace slag (GGBFS) is an amorphous by-product of the steel industry. It has a latent hydraulic reactivity, which can be catalyzed by proper activators to form cementitious materials. Alkali-activated slag (AAS) is one type of alkali-activated cement product that can offer superior properties over ordinary Portland cement (OPC) concrete, including high compressive strength at early age and excellent durability against chemical (acid, sulfate) attack (Shi, Roy, & Krivenko, 2005, 2005). In addition, AAS has lower CO_2 emissions than OPC, and its eco-friendly advantage mainly originates from utilization of by-products (Jiang, Chen, Rajabipour, & Hendrickson, 2014). However, some drawbacks of AAS still exist, which hinder its broad acceptation and industry application. One of the main disadvantages for potential applications of AAS in the construction industry is the volumetric instability, i.e., high shrinkage of AAS (Cartwright, Rajabipour, Radlińska, 2013a, 2014; Shi, Roy, & Krivenko, 2005).

Many researchers have reported that AAS exhibits significantly higher drying shrinkage than OPC (Bakharev, Sanjayan, & Cheng, 1999, 2000; Cartwright, Rajabipour, & Radlińska, 2013a, 2014; Cartwright, Rajabipour, Radlińska, 2013b; Collins & Sanjayan, 2000; Neto et al., 2008, 2008; Shi et al., 2005). For example, Cartwright, Rajabipour, and Radlińska (2014) measured the drying shrinkage of AAS mortar of four mixtures under 50% RH,

documenting that AAS has significantly higher drying shrinkage, finer pore structure, and lower stiffness than OPC. Collins and Sanjayan (2000) also observed the high shrinkage of AAS and related this phenomena to uniform pore size distribution in AAS. Similar experimental results and conclusions were also reported by Neto, Cincotto, and Repette (2008), who evaluated the shrinkage of AAS with different amounts of dissolved silica from activators. However, the scientific reasoning behind the high drying shrinkage behavior of AAS is still unknown. Some authors hypothesize that upon drying, a high capillary force forms in the materials of fine pore structures like AAS (Collins & Sanjayan, 2000; Neto et al., 2008). This assumption has not been verified though, as drying shrinkage tests under a broad range of relative humilities (e.g. from 30% RH to 100% RH) have not yet been conducted. Additionally, previous research merely observes the drying shrinkage of AAS under a constant relative humidity (50% RH in most cases). As such, this limited availability of experimental data prevents a more thorough understanding of the shrinkage behavior of AAS.

This paper presents the advanced drying shrinkage characterization of AAS mortar with various natures and dosages of activators. In particular, drying shrinkage of AAS is measured under two types of drying conditions, namely, rapid drying and step-wise drying, as explained later. Both of these drying conditions cover a broad range of relative humidities

from 30 to 85% RH. The objective of the present work is to contribute to the better understanding of drying shrinkage behavior of AAS and its associated underlying mechanism. The outcomes of this research can provide fundamental information on the shrinkage mechanism of AAS, and provide further insights into possible shrinkage reduction and mitigation strategies.

2.   EXPERIMENTAL PROCEDURE

2.1 Materials

A grade 120 (according to ASTM C989/C989M-13) GGBFS with a density of 2.89 g/cm^3 and a Type I Portland cement (according to ASTM C150/C150M-12) with a density of 3.14 g/cm^{3}were used in the present study. Table 1 shows the oxide composition of the aforementioned materials. When preparing the activating solutions, sodium hydroxide, sodium silicate solution, and distilled water were used. The sodium silicate solution ($Na_2O(SiO_2)_{1.6}(H_2O)_{10}$) had a specific gravity of 1.60 and pH of 13.7 at 20°C. The NaOH pellets had a specific gravity of 2.13. To prepare the activating solutions, reagent NaOH pellets were dissolved in water and covered in a closed beaker to avoid the loss of moisture and ingress of external CO_2. The solution was then shaken for 5 min and set aside for ~2 h to allow for heat dissipation. In addition, a small dosage of water-reducing admixture (WRA) was added to AAS systems to ensure adequate workability. Natural river sand (according to ASTM C33/C33M-13) was also used for each mixture. The sand had a fineness modulus of 2.60, oven-dry specific gravity of 2.52, and absorption capacity of 2.0%.

Table 1. Oxide compositions of slag and Portland cement (mass %).

	C	S	A	M	$\underline{S}$	F	N	K	LOI
Slag	47.5	30.8	11.45	3.65	3.03	1.81	0.17	0.38	1.17
Cement	62.5	19.9	5.44	2.31	4.93	2.26	0.30	0.89	0.86

Notes: C = CaO, S = SiO_2, A = Al_2O_3, M = MgO, F = Fe_2O_3, $\underline{S}$ = SO_3, H = H_2O, N = Na_2O, and K = K_2O.

2.2 Sample preparation

Four AAS mortars and a control OPC mortar were designed using a constant volumetric liquid (water + activator) to solid (slag or cement) ratio of 1.30. This resulted in an initial binder porosity of 56.5% in all five mixtures. For the control OPC mixture, the mass-based w/c was 0.414. For the AAS mixtures, the mass-based liquid to solid ratio was in the range of 0.489–0.510, depending on the concentration and density of the activating solutions. The details of mixture proportions are shown in Tables 2 and 3. In particular, mortars AAS1 (lower silica concentration) and AAS2 (higher silica concentration) were activated

using an alkaline solution that contained a combination of dissolved sodium hydroxide (NaOH) pellets, aqueous sodium silicate ($Na_2O(SiO_2)_{1.6}\cdot10H_2O$) (water glass), and water. Mortars AAS3 and AAS4 were activated solely by NaOH in water (either 2M or 4M). It should be mentioned here that the amount of water reported in Table 2 accounts for the absorption of oven-dried sand.

Table 2. Mortar mixture proportions (in grams per liter of mortar).

Mix ID	NaOH	Na_2O $(SiO_2)_n$	Water*	Cement	Slag	Sand
OPC	0	0	296.8	657	0	1247
AAS1	23.77	35.70	263.6	0	604	1247
AAS2	5.94	95.49	234.6	0	604	1247
AAS3	23.77	0	285.9	0	604	1247
AAS4	47.54	0	274.8	0	604	1247

Note: Water content accounts for sand absorption.

Table 3. Activating solution properties for AAS mixtures.

Mix ID	SiO_2/Na_2O	pH	Density (g/cc)	WRA (cc/kg)
AAS1	0.41	14.31	1.09	5.00
AAS2	1.22	13.78	1.13	2.00
AAS3	0	14.30	1.04	4.15
AAS4	0	14.60	1.09	8.00

To evaluate shrinkage deformation, a series of "mini-bar" prism samples (1.27 cm × 1.27 cm × 12.7 cm) was cast in this study. The smaller dimension of the samples allowed the systems to reach equilibrium in a relatively short period of time. A PVC mold with a gage length of 4″ was used in samples preparation. All samples were dried in nitrogen purged Vena VC-10 environmental chambers.

2.3 Testing procedure

To evaluate the effect of drying rate on shrinkage behavior of AAS, two types of experimental procedures were utilized, namely, rapid drying and step-wise drying. Rapid drying involved measuring shrinkage at constant RH until equilibrium was reached, while step-wise drying measured shrinkage across a broad range of RH. In particular, environmental chambers were programed for four different humidities (85, 70, 50, and 30% RH) at constant temperature (23 ± 0.5°C). The rapid drying shrinkage was measured for all five mixtures (four samples per mixture) at each constant relative humidity under dry nitrogen (N_2) purge, after 7 days of moist curing (100% RH, 23 ± 0.5°C). The concentration of CO_2 in environmental chambers was periodically measured with a portable CO_2 analyzer and was found to be 0 ppm. In case of step-wise drying procedure, the

specimens were dried initially at 85% RH until they reached equilibrium, at which point, the humidity was dropped to 70%. Subsequent RH reductions to 50 and 30% RH occurred after specimens came to equilibrium at each RH step. Length measurements were taken through a modified digital comparator with an invar reference bar. The accuracy of length measurements was 0.0001″. Simultaneous mass measurements were taken using a high precision balance with an accuracy of 0.01 g.

3. EXPERIMENTAL RESULTS

3.1 Rapid drying shrinkage of AAS

Figure 1 shows the results of the measured rapid drying shrinkage of all five mortar mixtures during the first 30 days of testing. All AAS mixtures show higher drying shrinkage strains than the control OPC mixture at all relative humidities except for AAS3 at 30% RH.

OPC shows increasing shrinkage with a decreasing relative humidity, which is consistent with the findings of other authors (Baroghel-Bouny, Mounanga, Khelidj, Loukili, & Rafaï, 2006; Hansen, 1987). In contrast, the AAS mixtures show more complicated drying shrinkage behavior, where the largest ultimate drying shrinkage of AAS3 and AAS4 is observed at 70% RH. Similarly, AAS1 and AAS2 shrink the most at 50% RH, even though all mixtures were also dried to 30% RH.

Figure 2 represents the mass loss data for the four AAS and the control OPC mixtures. It can be seen that for all mixtures, a lower RH promotes higher moisture loss. Furthermore, moisture loss of each AAS mixture is larger than that for OPC. This contradicts with the findings of Collins and Sanjayan (2000), who measured lower mass loss upon drying for AAS than for OPC. At each relative humidity, AAS3 showed the highest mass loss. This is likely due to the coarse porosity of the paste in AAS3. The moisture loss for the other three AAS mixtures was measured to be similar.

3.2 Step-wise drying shrinkage

The second series of experiments involved drying samples to equilibrium and then gradually dropping the RH. Figures 3 and 4 display the step-wise drying shrinkage and mass loss results of all five mortar mixtures. Similar to rapid drying, the control OPC showed the lowest drying shrinkage and mass loss among all mixtures evaluated. It can be seen that when dried gradually, the relationship between shrinkage and relative humidity for AAS materials differs significantly from that observed under rapid drying. Generally, drying shrinkage of all AAS samples exposed to step-wise procedure showed relatively higher values than those measured in the case of rapid drying. It should be noted here that ultimately

all samples were dried until they reached equilibrium at 30% RH. Comparing rapid and step-wise drying of AAS3, it can be seen that when dried gradually to a relative humidity of 50%, AAS3 shows 77% higher shrinkage deformations than when dried rapidly to the same RH. Similar tendencies are observed for the other AAS mixtures. All mixtures had slightly lower mass loss during the step-wise drying as compared to the direct drying process. As such, it can be concluded that drying shrinkage behavior of AAS materials is highly dependent on the rate of drying.

4. DISCUSSION

According to the Mackenzie–Bentz equation (Bentz, Garboczi, & Quenard, 1998), one can calculate the ultimate paste shrinkage due to capillary stresses (P_{cap}) induced by drying:

$$\varepsilon_\rho = \frac{S}{3} P_{cap} \left[\frac{1}{K} - \frac{1}{K_s} \right] \tag{1}$$

where S corresponds to the volumetric degree of saturation, K is the bulk elastic modulus of the paste (as shown in Table 4), and K_s is the bulk modulus of the solid skeleton (e.g., C–S–H or unreacted solids). It can be seen that the material parameters controlling the calculated strain include the degree of saturation, effective bulk modulus, and skeleton modulus (Bentz et al., 1998; Cartwright et al., 2014). Capillary pressure is similar at the same RH according to Kelvin equation (Equation (2)).

$$P_{cap} = -\rho_1 \frac{RT}{M_1} \ln\left(RH\right) \tag{2}$$

where P_{cap} is the capillary pressure, ρ_1 is density of liquid, M_1 is molecular mass and assumed to be same with pure water, R = 8.314 [J/(mol K)] is the universal gas constant, and T is temperature [K].

Additionally, a recent study also showed that the skeleton stiffness (K_s) of AAS is similar to that of OPC (Gebregziabiher & Peethamparan, 2013).

A higher shrinkage of AAS may originate from a higher degree of saturation and lower bulk modulus. As shown in Figure 5, the measured degree of saturation for OPC is slightly higher than that for OPC for each RH at equilibrium. The effective capillary stress (i.e., SP_{cap}) can be calculated and is shown in Figure 6. It should be noted that the capillary stress theory is primarily valid for RH > 60% (~) as a liquid–vapor meniscus cannot form in pores smaller than those that correspond to RH <60%. It can be seen in Figure 6 that the effective capillary stress of OPC is slightly higher than that of AAS. This would eliminate a higher degree of saturation as a primary cause of higher shrinkage of AAS. Thus,
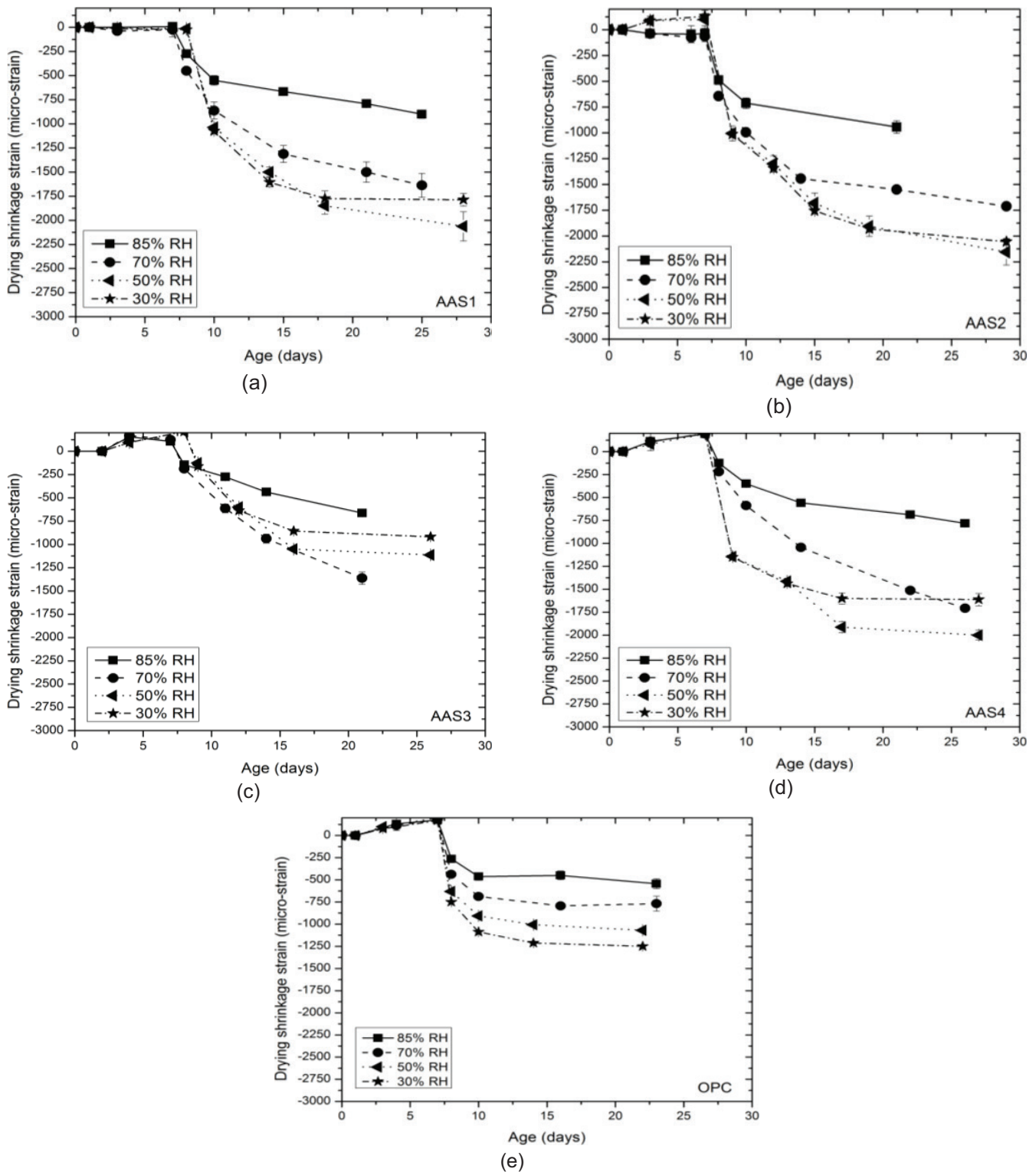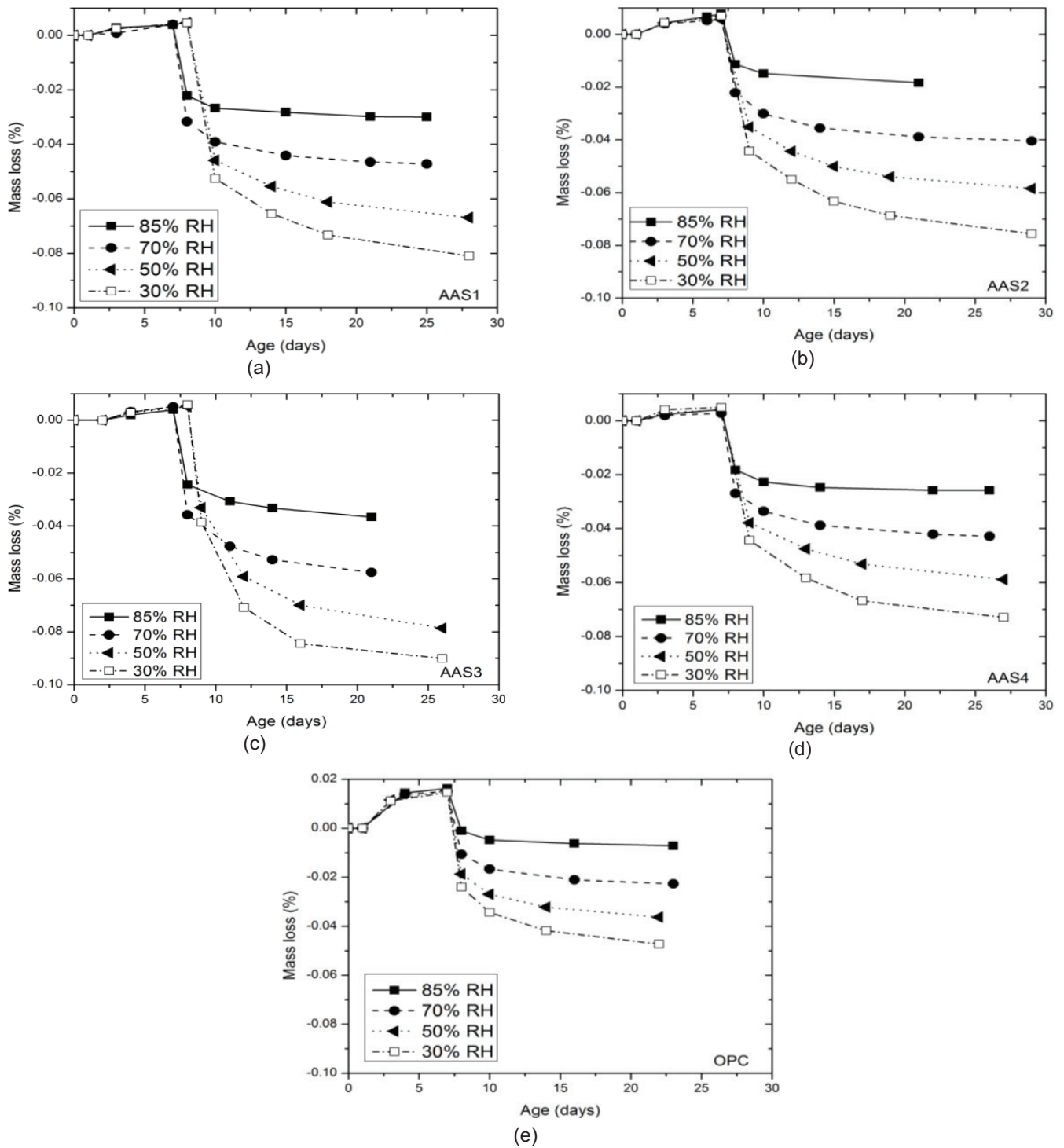
Figure 1. Rapid drying shrinkage under nitrogen purge for all mortar mixtures (a) AAS1; (b) AAS2; (c) AAS3; (d) AAS4; (e) OPC (after 7 days moist curing).

the larger drying shrinkage of AAS could result from a lower stiffness. As shown in Table 4, AAS3 and AAS4 mortars have ~33% lower stiffness, but the stiffness values of AAS1 and AAS2 are similar, or even higher than that of OPC. Therefore, the value of stiffness itself may partially explain the higher

shrinkage of AAS3 and AAS4, but cannot properly explain the high shrinkage performance of AAS1 and AAS2. Therefore, the capillary pressure theory, at least for AAS1 and AAS2, cannot explain the high shrinkage performance of AAS by itself and its strong dependence on drying rate.

Figure 2. Mass loss under rapid drying (nitrogen purged) for all mortar mixtures: (a) AAS1; (b) AAS2; (c) AAS3; (d) AAS4; (e) OPC (after 7 days moist curing).

On the other hand, Equation (1) assumes a linear elastic behavior and does not account, for example, for creep. Creep is a phenomenon that results in the gradual increase in deformation under a constant stress. As shown in Figures 1 and 2, the mass loss of AAS plateaus is much faster than that of shrinkage. This means that AAS mixtures continue to shrink even

though they are not losing any more water. This may suggest significant creep deformation in AAS, while for OPC, the shrinkage practically ceases when moisture loss reaches equilibrium. This is strong evidence that creep plays a significant role in drying shrinkage of AAS.

The correlation between relative humidity and drying shrinkage for all five mortar mixtures subjected to
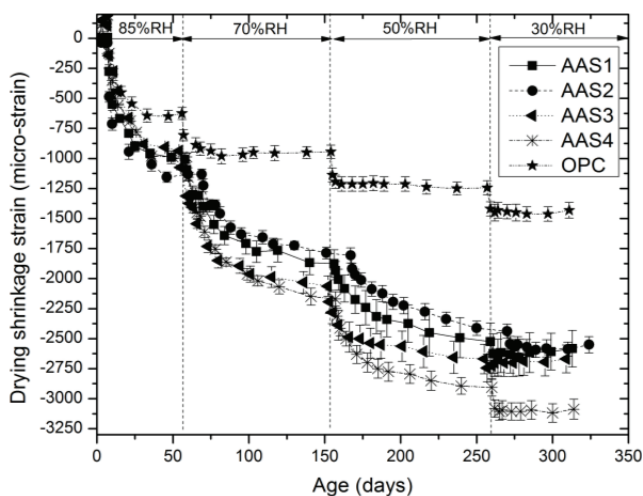
Figure 3. Step-wise drying shrinkage results for all five mortar mixtures.
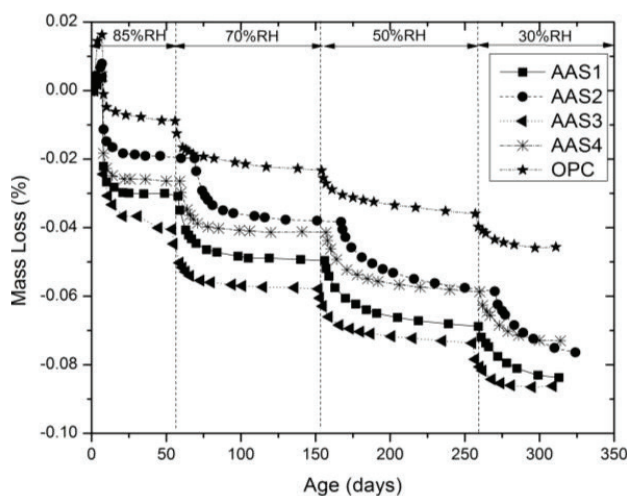

Figure 4. Step-wise drying moisture loss results for all five mortar mixtures.

Table 4. Bulk modulus of elasticity K of mortars at 28 days.

Mix ID	Bulk modulus (GPa)
AAS1	11.34
AAS2	10.63
AAS3	6.96
AAS4	7.42
OPC	9.44

Note: Each data point is an average of two duplicate cylindrical specimens.

rapid drying procedure has been shown in Figure 7. It can be seen that the OPC mixture shows a bi-linear relationship, while AAS mixtures show a parabolic relationship between ultimate shrinkage and relative humidity. Particularly, AAS1 and AAS2 showed the highest shrinkage at 70% RH, while AAS3 and AAS4 showed the highest shrinkage at 50% RH. This unique phenomenon notably demonstrates the influence of drying rate on shrinkage behaviors of AAS.

Interestingly, when dried under the step-wise process, the shrinkage behavior of AAS differs significantly as compared to rapid drying, where the highest drying shrinkage deformations were observed at the lowest relative humidity. This may be due to the formation of permanent shrinkage strains (e.g., creep) during the gradual drying process.

It is possible that other shrinkage driving forces, (e.g., Gibbs–Bangham strain) play important roles in shrinkage behavior of AAS, since the notably dependent shrinkage behavior of AAS on drying rate cannot be completely explained in present studies. The investigation of the shrinkage mechanisms of AAS is currently a main research focus at Pennsylvania State.
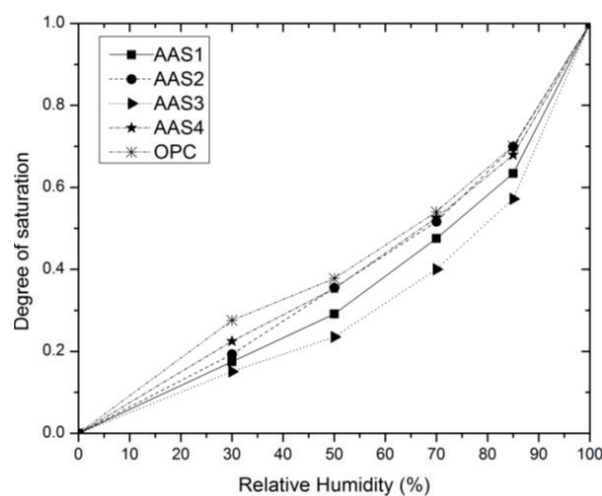

Figure 5. The correlation between relative humidity and degree of saturation at equilibrium for all five mortar mixtures.
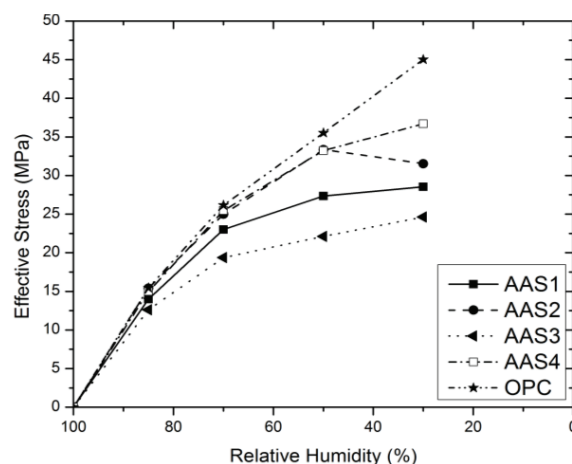

Figure 6. The correlation between relative humidity and drying shrinkage for all five mortar mixtures.
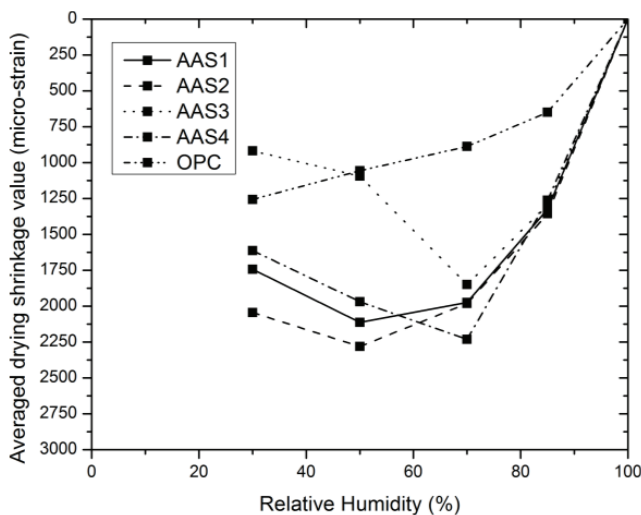
Figure 7. The correlation between relative humidity and drying shrinkage for all five mortar mixtures.

5. CONCLUSIONS

In this article, the influence of drying rate on shrinkage characteristics of AAS was studied. In particular, four AAS mortar mixtures and one control OPC mortar were exposed to different drying procedures, namely, rapid drying and step-wise drying. For rapid drying, four different relative humidities (i.e., 30, 50, 70, and 85% RHs) were utilized to investigate the shrinkage behavior of AAS. In step-wise drying scenario, a gradual change of RH from 85 to 30% RH was applied.

The following conclusions can be drawn according to the experimental results and analysis:

(1) AAS mixtures have a unique parabolic relationship between relative humidity and ultimate drying shrinkage that differs significantly from the bi-linear correlation found in OPC mixtures.

(2) Drying rate significantly affects the drying shrinkage behavior of AAS mortars.

(3) Creep deformation seems to contribute significantly to drying shrinkage of AAS.

(4) Effective capillary stress (SP_{cap}) was estimated to be slightly higher for OPC than for AAS and cannot explain the high shrinkage of AAS.

(5) The stiffness of mixtures activated by NaOH is smaller than that of OPC and contributes to their high shrinkage deformations.

REFERENCES

Bakharev, T., Sanjayan, J., & Cheng, Y.-B. (2000). Effect of admixtures on properties of alkali-activated slag concrete. *Cement and Concrete Research, 30*, 1367–1374.

Bakharev, T., Sanjayan, J.G., & Cheng, Y.-B. (1999). Alkali activation of Australian slag cements. *Cement and Concrete Research, 29*, 113–120.

Baroghel-Bouny, V., Mounanga, P., Khelidj, A., Loukili, A., & Rafaï, N. (2006). Autogenous deformations of cement pastes: Part II. W/C effects, micro–macro correlations, and threshold values. *Cement and Concrete Research, 36*, 123–136.

Bentz, D. P., Garboczi, E. J., & Quenard, D. A. (1998). Modelling drying shrinkage in reconstructed porous materials: Application to porous Vycor glass. *Modelling and Simulation in Materials Science and Engineering, 6*, 211.

Cartwright, C., Rajabipour, F., & Radlińska, A. (2013a). Shrinkage characteristics of alkali-activated slag cements. *3rd International Conference on Sustainable Construction Materials and Technology – SCMT2013*, Ktoto, Japan.

Cartwright, C. P., Rajabipour, F., & Radlińska, A. (2013b). Measuring the chemical shrinkage of alkali-activated slag cements using the buoyancy method, mechanics and physics of creep, shrinkage, and durability of concrete: a tribute to Zdenek P. Bažant. *Proceedings of the Ninth International Conference on Creep, Shrinkage, and Durability Mechanics (CONCREEP-9)*, September 22–25, 2013, Cambridge, MA. ASCE Publications, p. 308.

Cartwright, C., Rajabipour, F., & Radlińska, A. (2014). Shrinkage characteristics of alkali-activated slag cements. *ASCE Journal of Materials in Civil Engineering* (accepted).

Collins, F., & Sanjayan, J. (2000). Effect of pore size distribution on drying shrinking of alkali-activated slag concrete. *Cement and Concrete Research, 30*, 1401–1406.

Gebregziabiher, B. S., & Peethamparan, S. (2013). Characterization of alkali activated slag gel using nano-indentation. *3rd International Conference on Sustainable Construction Materials and Technology – SCMT2013*, Ktoto, Japan.

Hansen, W. (1987). Drying shrinkage mechanisms in Portland cement paste. *Journal of the American Ceramic Society, 70*, 323–328.

Jiang, M., Chen, X., Rajabipour, F., & Hendrickson, C. T. (2014). Comparative life cycle assessment of conventional, glass powder, and alkali-activated slag concrete and mortar. *Journal of Infrastructure Systems*.

Neto, A. A. M., Cincotto, M. A., & Repette, W. (2008). Drying and autogenous shrinkage of pastes and mortars with activated slag cement. *Cement and Concrete Research, 38*, 565–574.

Shi, C., Roy, D., & Krivenko, P. (2005). *Alkali-activated cements and concretes*. London: Taylor & Francis.